

Applicability of flashing desalination technique for small scale needs using a novel integrated system coupled with nanofluid-based solar collector



A.E. Kabeel*, Emad M.S. El-Said

Mechanical Power Engineering Department, Faculty of Engineering, Tanta University, Tanta, Egypt

HIGHLIGHTS

- An attempt for the application of flash desalination technique for small scale needs is introduced.
- A nano-fluid is used as a working fluid for solar has been made to enhance the heat transfer rate.
- The proposed system gives a reasonable production of fresh water up to 7.7 l/m²/day under the operation conditions.
- The estimated cost of the generated potable water was 11.68 US\$/m³.

ARTICLE INFO

Article history:

Received 5 April 2013

Received in revised form 17 September 2013

Accepted 11 November 2013

Available online 11 December 2013

Keywords:

Flashing desalination

Solar collector

Nano-fluid

ABSTRACT

The present study introduces an attempt for the application of flash desalination technique for small scale needs. An integrated system uses a flashing desalination technique coupled with nano-fluid-based solar collector as a heat source has been made to investigate both the effect of different operating modes and that of the variation of functioning parameters and weather conditions on the fresh water production. The flashing unit is performed by similar construction design technique of commercial multi-stage flashing (MSF) plant. The thermal properties of working fluid in the solar collector have been improved by using different concentrated nano-particles. Cu nano-particle is used in the modeling to determine the proper nano-fluid volume fraction that gives higher fresh water productivity. An economic analysis was conducted, since it affects the final cost of produced water, to determine the cost of fresh water production. Although a system may be technically very efficient, it may not be economical. The effect of different feed water and inlet cooling water temperatures on the system performance was studied. The mathematical model is developed to calculate the productivity of the system under different operating conditions. The proposed system gives a reasonable production of fresh water up to 7.7 l/m²/day under the operation conditions. Based on the cost of energy in Egypt, the estimated cost of the generated potable water was 11.68 US\$/m³. The efficiency of the system is measured by the gained output ratio (GOR) with day time. The gained output ratio (GOR) of the system reaches 1.058. The current study showed that the solar water heater collecting area is considered a significant factor for reducing the water production cost. Also, the produced water costs decrease with increasing the collecting area of the solar water heater. The volume fractions of nano-particle in solar collector working fluid have a significant impact on increasing the fresh water production and decreasing cost.

© 2013 Elsevier B.V. All rights reserved.

1. Introduction

Fresh water demand is persistently increasing both as populations around the world keep growing and as existing fresh water reserves keep declining due to consumption and pollution. Energy demand is also continually increasing due to relentless global industrialization. Oil and gas remain the primary sources of energy for most of the world; however, their reserves are dwindling, production is peaking, and consumption is harming the environment. The electricity demand

is forecasted to be increased during the next decades, especially in the developing countries. The large scale implementation of the standard high-capacity desalination methods faces numerous technological, economic and policy barriers, and they are not used in decentralized regions with a poor infrastructure due to their permanent need of qualified maintenance and electricity supply. Solar thermal production technologies are promising, though they are expected to be able to satisfy good part of future desalination need. So, desalination units driven by solar energy are a suitable choice for the production of fresh water in remote and sunny regions. In concept, large scale desalination technique based MSF and MED system applications for small scale solar desalination needs are similar to conventional thermal desalination systems. The main difference is that in the former, solar energy collection devices are used. Some proposals use centralized, concentrating

* Corresponding author. Tel.: + 20 1001543587.

E-mail addresses: kabeel6@hotmail.com (A.E. Kabeel), emad_mech@hotmail.com (E.M.S. El-Said).

solar power at a high receiver temperature to generate hot water. Thermodynamically, flash evaporation occurs when a saturated liquid undergoes a sudden reduction in the surrounding pressure so that a part of the liquid immediately turns to vapor to regain equilibrium; under adiabatic conditions, the generated vapor receives its latent heat of vaporization at the expense of the surrounding liquid and both the vapor and the residual liquid are cooled to the saturation temperature at the reduced pressure. Nafey et al. [1] investigated theoretically and experimentally a small unit for water desalination by solar energy and a flash evaporation process at different real environmental conditions. The system consists of a solar water heater (flat plate solar collector) working as a brine heater and a vertical flash unit that is attached with a condenser/preheater unit. The mathematical model is developed to calculate the productivity of the system under different operating conditions. Comparisons between the theoretical and experimental results are performed. The average accumulative productivity of the system ranged between 1.04 and 1.45 kg/day/m². The average summer productivity ranged between 5.44 and 7 kg/day/m² and 4.2 and 5 kg/day/m². Baig et al. [2] investigated the effect of various operating conditions on the performance ratio, brine temperature and salinity as it leaves the last flash stage in a once-through the multi-stage flash (MSF) distillation system. They use reliable correlations for calculating brine properties that vary with both temperature and salinity. They compared the numerical results obtained with the published data on similar plants. A sensitivity analysis to identify the key parameters that significantly influence on the desalination plant performance is carried out in an attempt to contribute a better understanding on modeling and optimum operation of MSF desalination processes. Both analytical solutions and experimental/field analysis were required to identify the most influential parameters that affect the performance and set proper plans for performance optimization. To accurately estimate the variables related to the brine heater, selecting the proper number of stages and the stage-to-stage temperature drop is of crucial importance. The thermal properties dependent on the operating conditions may affect the accuracy of numerical results. The salinity of the feed seawater has a significant effect on the plant characteristics. Junjie et al. [3] studied experimentally the heat and mass transfer properties of static/circulatory flash evaporation, i.e., nonequilibrium fraction (NEF), evaporated mass and heat transfer coefficient. The heat transfer coefficient was redefined as average heat flux released from unit volume of water film under unit superheat. The results indicated that this coefficient has a time-dependent function and a peak value existed at its evolution versus time. Saad et al. [4] proposed and designed a new desalination system for converting sea water into fresh water utilizing the waste heat of internal combustion engines. The desalination process is based on the evaporation of sea water under a very low pressure (vacuum). The low pressure is achieved by using the suction side of a compressor rather than a commonly used vacuum pump. The evaporated water is then condensed to obtain fresh water. The effects of operational variables such as evaporator temperature, condenser temperature, vacuum pressure, and flow rate of both evaporator and condenser on the yield of fresh water are experimentally investigated. It is found that decreasing the vacuum pressure causes a significant increase in the yield of fresh water. It is also found that decreasing the condenser temperature, or increasing the evaporator temperature leads to an increase in the yield of fresh water. Moreover, increasing the condenser flow rate tends to increase the yield of fresh water. The same trend is attained by increasing the evaporator flow rate. Abutayeh and Goswami [5] simulated theoretically and experimentally a passive vacuum flash desalination system. The system consists of a saline water tank, a concentrated brine tank, and a fresh water tank placed on a ground level plus an evaporator and a condenser located several meters above the ground. The evaporator–condenser assembly, or flash chamber, is initially filled with saline water that later drops by gravity, creating a vacuum above the water surface in the unit without a vacuum pump. The vacuum is maintained by the internal hydrostatic pressure balanced by the atmospheric

pressure. The ground tanks are open to the atmosphere, while the flash chamber is insulated and sealed to retain both heat and vacuum. The simulation results showed that running the system at higher flash temperatures with a fixed flash chamber size resulted in faster vacuum erosion leading to less overall evaporation.

Asirvatham et al. [6] studied experimentally the steady state convective heat transfer of de-ionized water with a low volume fraction (0.003% by volume) of copper oxide (CuO) nano-particles. The results have shown 8% enhancement of the convective heat transfer coefficient of the nano-fluid even with a low volume concentration of CuO nano-particles. The heat transfer enhancement was increased considerably as the Reynolds number increased.

Yousefi et al. [7] investigated experimentally the effect of Al₂O₃/water nano-fluid, as working fluid, on the efficiency of a flat-plate solar collector. The weight fraction of nano-particles was 0.2% and 0.4% and the particle dimension was 15 nm. The mass flow rate of nano-fluid varied from 1 to 3 l/min. The results showed that, in comparison with water as absorption medium using the nano-fluids as working fluid increases the efficiency. For 0.2 wt.% the increased efficiency was 28.3%.

Banat and Jwaied presented an economic assessment performed to estimate the expected water cost, which is the ultimate measure of the feasibility of the two solar powered stand-alone membrane distillation units (compact and large) [8].

Kabeel et al. [9] introduced an economic analysis of a small scale desalination plant based on two different technologies; the first technology is air humidification – dehumidification process while the second one is the water flashing evaporation process. The total cost of ownership (TCO) concept was adopted in the analysis.

Mabrouk [10] presented a technoeconomic comparison between once through long tube (MSF-OT-LT) with atmospheric deaerator, and brine recycle cross tube (MSF-BR-CT) evaporators.

The novelty and contribution in the proposed system can be summarized in the following points:

- Study the applicability of (MSF) multi-stages flashing desalination technology and design in small-scale water production.
- Development of solar collector water heaters using nano-fluid (Cu/water) as a heating source for desalination system in continuous conditions.

The current work aims to introduce an attempt for the application of flash desalination technique for a small scale needs. A pilot unit was theoretically designed and analyzed to insure;

- Quasi-steady theoretical analysis of desalination system for predictive modeling of small-scale single stage flash (SSF).
- Performance and economical analysis of SSF desalination system.
- Studying the possible factors and parameters those have an effect on the system production and cost.

2. System Process Description

The solar SSF unit consists of flashing chamber, condenser, mixing tank, solar water heater and helical heat exchanger as shown in Fig. 1. The water at (3) is pumped to the flashing chamber to be evaporated suddenly through flashing. The extracted water vapor on flashing chamber is flowed to the condenser. The saline cooling water at (6) is fed to the flashing unit condenser to condense the water vapor and exit at (7). A part of saline water at (7) is flowed to helical heat exchanger to backup water inside the closed loop at (11) while the rest is drained at (10). The desalinated water at (8) is collected from the bottom of the condenser tray, while is rejected from the bottom of the condenser tray. The flashing evaporation depends on the pressure reduction. So, the inside the condenser and flashing chamber is vacuumed by using vacuum pump at (9).

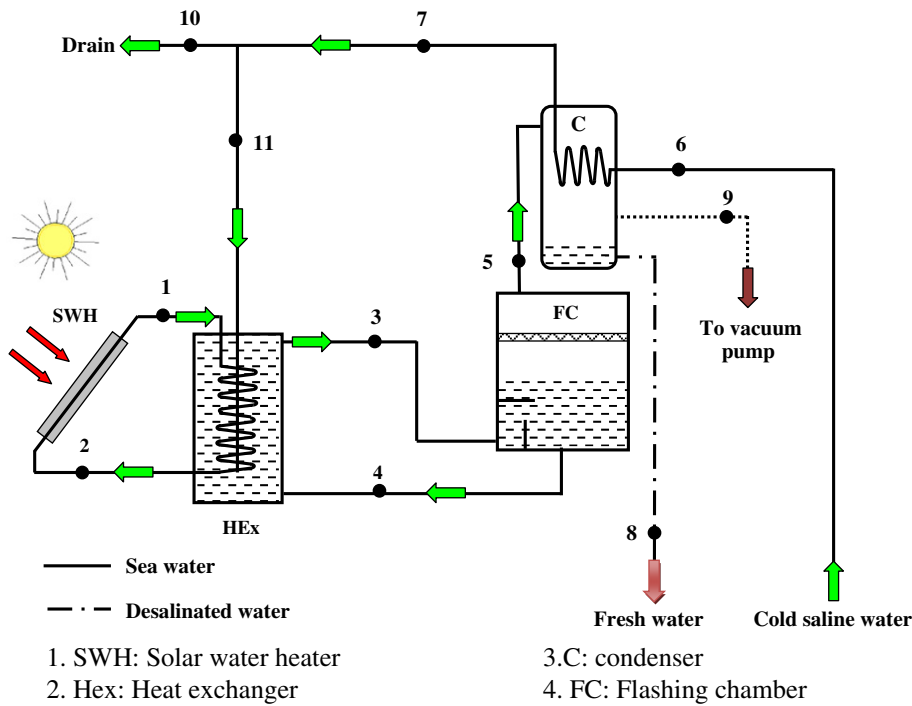


Fig. 1. Schematic diagram of (SSF) system.

Then, the brine reject from flashing chamber at (4) is returned to heat exchanger (Hex). As a result of the saline water flow in a closed loop between the flashing chamber and helical heat exchanger the water salinity will increase with time. So when the level of water salinity reaches a certain value a quantity of high-salinity water will discharge from the loop and replaced by an amount of low-salinity water exit form condenser at (11).

Description of the equipments of the system is shown in Table 1.

3. System Mathematical Modeling

A steady-state mathematical model is developed to allow the determination of coupling equations between the water temperature and water content inside each component. The water salinity will be considered. For the energy balance and governing equations for each of the system components the following assumptions are considered:

1. The system is behaved of a quasi-steady-state manner and one dimensional; i.e. the variables, while varying from hour to hour, are

considered constant during every hour of analysis and the unsteady terms in the governing equations are neglected.

2. Heat losses from the edges of the solar water heaters, mixing tank, and flashing unit to the ambient are neglected (i.e. the heat exchanger outside walls are adiabatic).
3. Negligible conduction resistance in glass covers of solar collectors.
4. The absorption of solar radiation in the cover is neglected insofar as it affects loss from the solar water collector.
5. The temperature distribution over every cross section in the mixing tank is uniform.
6. The nano-fluid composition is water and Cu only.
7. There are no phase changes (condensation or vaporization) in the fluid streams flowing through the heat exchanger.
8. The distillate product is salt free.
9. The flash chamber is in equilibrium with the brine leaving the stage.
10. The distillate vapor always condenses completely.
11. The flow of non-condensable gases is negligible.

The energy balance equation can be written for the entire system in the following manner, by taking input energy terms equal to output energy terms:

Table 1
System technical specifications data used for the simulation.

Technical specifications and operation data	Value
Water heater solar collector	
Total aperture area, m ²	7.075
Glass type low iron glass thickness, mm	3
Collector insulation Fiberglass sides thickness, mm	30
Fiberglass back thickness, mm	50
Nano-particles size, mm	30×10^{-6}
Heat exchanger	
Exchange surface area, m ²	1.37
Flashing chamber	
Size, m	$0.2 \times 0.5 \times 0.5$
Brine pool height, m	0.10
Condenser surface area, m ²	0.2
Condenser	
Size, mm	$186 \times 144 \times 260$
Exchange surface area, m ²	0.1

3.1. Flat plate solar water heater

Flat plate solar collector as shown in Fig. 2 is used to heat water. Under steady-state conditions, the useful rate of heat delivered by a solar collector is equal to the rate of energy absorbed by the heat transfer nano-fluid minus the direct or indirect heat losses from the surface to the surroundings. The model solves the energy balance of the solar collector under steady-state conditions according to the modeling equations in [11].

The energy conducted to the region of the tube per unit length in the flow for both sides is given by:

$$q_p' = (W_{tube} - d_{wc,o}) F [S - U_{L,wc} (T_{wc,p} - T_{am})] \quad (1)$$

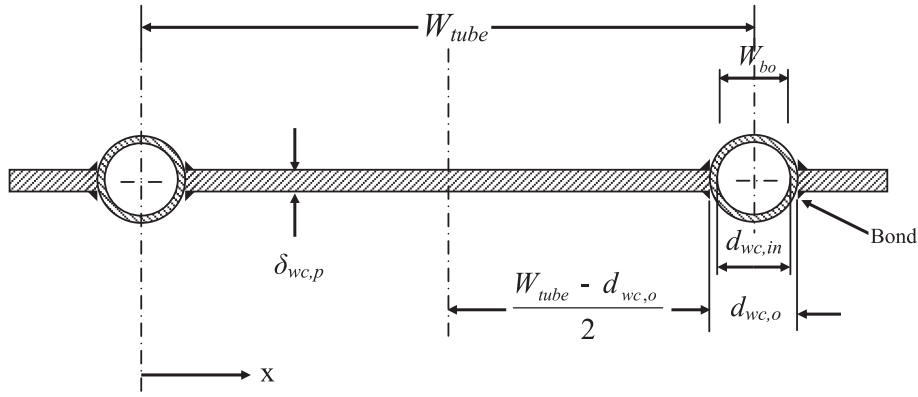


Fig. 2. Sheet and tube dimensions of flat plate solar collector.

Where fin efficiency (F) is given by:

$$F = \frac{\tanh \left[\Gamma (W_{tube} - d_{wc,o}) / 2 \right]}{\Gamma (W_{tube} - d_{wc,o}) / 2} \quad (2)$$

The useful gain of the collector is also including the energy collected above the tube region. This is given by

$$\dot{q}'_{tube} = d_{wc,o} [S - U_{L,wc} (T_{wc,p} - T_{am})] \quad (3)$$

Accordingly, the useful energy gain per unit length in the direction of the fluid flow is calculated as follows:

$$\dot{q}'_u = \dot{q}'_p + \dot{q}'_{tube} = [(W_{tube} - d_{wc,o}) F + d_{wc,o}] [S - U_{L,wc} (T_{wc,p} - T_{am})] \quad (4)$$

This energy ultimately must be transferred to the fluid, which is expressed in terms of two resistances as follows:

$$\dot{q}'_u = \frac{T_{wc,p} - T_{nf,wc}}{\frac{1}{h_{nf,wc,in} \pi d_{wc,in}} + \frac{1}{C_{bo}}} \quad (5)$$

In Eq. (4), C_{bo} is the bond conductance, which can be estimated from knowledge of the bond thermal conductivity, (K_{bo}), the average bond thickness, (δ_{bo}), and the bond width, (W_{bo}). The bond conductance on a per unit length basis is given by

$$C_{bo} = \frac{K_{bo} W_{bo}}{\delta_{bo}} \quad (6)$$

To obtain an expression for the useful gain in terms of known dimension, physical parameters, and fluid temperature, ($T_{nf,wc}$) must eliminate. So, Solving Eq. (4) for, ($T_{wc,p}$), substituting it into Eq. (3), and solving the resultant equation for the useful gain, we get

$$\dot{q}'_u = W_{tube} F' [S - U_{L,wc} (T_{nf,wc} - T_{am})] \quad (7)$$

Where the collector efficiency factor (F') is given by:

$$F' = \frac{1}{U_{L,wc} \left\{ \frac{1}{U_{L,wc} [d_{wc,o} + F (W_{tube} - d_{wc,o})]} + \frac{1}{C_{bo}} + \frac{1}{h_{nf,wc,in} \pi d_{wc,in}} \right\}} \quad (8)$$

By the consideration of an infinitesimal length (dy) of the tube. The useful energy delivered to the fluid is $q'_u dy$. Under steady-state conditions, an energy balance for n tubes gives:

$$\dot{q}'_u dy + \frac{\dot{m}_{nf,wc}}{N_{wc,tube}} C_{p,nf} T_{nf,wc} - \frac{\dot{m}_{nf}}{N_{wc,tube}} C_{p,nf} \left(T_{nf,wc} + \frac{dT_{nf,wc}}{dy} dy \right) = 0 \quad (9)$$

Dividing the above equation by (dy), finding the limit as (dy) approaches 0, and substituting Eq. (7) results in the following differential equation:

$$\dot{m}_{nf,wc} C_{p,nf} \frac{dT_{nf,wc}}{dy} - N_{wc,tube} W_{tube} F' [S - U_{L,wc} (T_{nf,wc} - T_{am})] = 0 \quad (10)$$

Assuming variables F' , $U_{L,wc}$, and $C_{p,nf}$ to be constants and performing the integration gives:

$$\ln \left(\frac{T_{nf,wc,o} - T_{am} - (S/U_{L,wc})}{T_{nf,wc,in} - T_{am} - (S/U_{L,wc})} \right) = - \frac{N_{wc,tube} W_{tube} L_{coil,wc} F' U_{L,wc}}{\dot{m}_{nf,wc} C_{p,nf}} \quad (11)$$

Where

$$A_{wc} = N_{wc,tube} W_{tube} L_{tube,wc}$$

Substituting by (A_{wc}) in Eq. (11), the following equation is obtained

$$\frac{T_{nf,wc,o} - T_{am} - (S/U_{L,wc})}{T_{nf,wc,in} - T_{am} - (S/U_{L,wc})} = \exp \left(- \frac{A_{wc} F' U_{L,wc}}{\dot{m}_{nf,wc} C_{p,nf}} \right) \quad (12)$$

Then

$$T_{nf,wc,o} = [T_{nf,wc,in} - T_{am} - (S/U_{L,wc})] \left[\exp \left(- \frac{A_{eff} F' U_{L,wc}}{\dot{m}_{nf,wc} C_{p,nf}} \right) \right] + T_{am} + (S/U_{L,wc}) \quad (13)$$

The heat transfer coefficient of nono-fluid in Eq. (8) ($h_{nf,wc,in}$) inside the solar collector of tubes can determined using experimental correlations are given in the Appendix A.

3.2. Single stage flashing unit

The mathematical model for the single flash unit is simply introduced. It includes heat and salt mass balances, rate equations for the heat transfer units, as well as energy balances for the condenser.

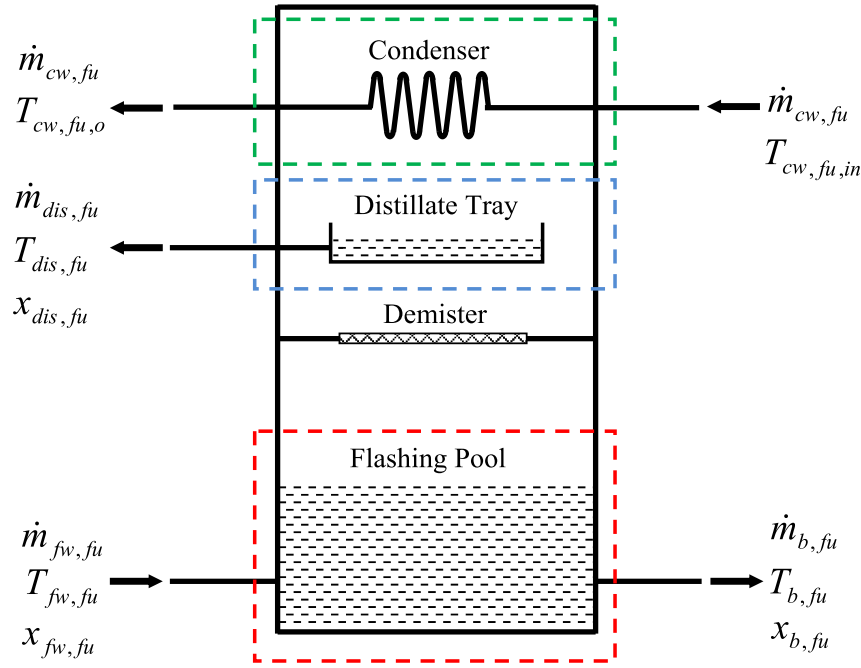


Fig. 3. Single stage flash desalination unit.

3.2.1. Flashing pool model

Fig. 3 shows the schematic diagram of the flashing pool section, the mass and heat balances are given as followed:

Total mass and salt mass balances:

$$\dot{m}_{fw, fu} = \dot{m}_{b, fu} + \dot{m}_{dis, fu} \quad (14)$$

$$x_{fw, fu} \dot{m}_{fw, fu} = x_{b, fu} \dot{m}_{b, fu} \quad (15)$$

Eq. (15) assumes that the salt concentration, (x_{dw}), in the formed vapor is zero.

3.2.2. Energy balance

The energy balance for the flashing brine is expressed as follows:

$$\dot{m}_{fw, fu} i_{fw, fu} = \dot{m}_{b, fu} i_{b, fu} + \dot{m}_{dis, fu} \lambda_{v, fu} \quad (16)$$

The brine is assumed to leave the flashing pool at saturation condition, and is calculated as a function of temperature and salinity of the exit brine conditions.

3.2.3. Condenser tube bundle model

The flashed brine vapor and flashed distillate vapor are flowed over the tube bundle to be condensed, where the condensate flows back to the distillate tray. The effect of pressure loss over the tube bundle on the heat transfer coefficient was neglected in this model. However, the effect of the pressure loss across the tube bundle on the energy balance was considered in the form of temperature drop. The condensate was considered as a saturated liquid. The effect of condensate sub-cooling on the energy balance was evaluated as function of sub-cooling temperature.

3.2.4. Energy balances

$$\dot{m}_{dis, fu} \lambda_{v, fu} = \dot{m}_{cw, fu} (i_{cw, o, fu} - i_{cw, in, fu}) + \dot{m}_{dis, fu} i_{dis, fu} \quad (17)$$

3.2.5. The heat transfer rate equation for the condenser is

$$\begin{aligned} \dot{m}_{cw, fu} (i_{cw, o, fu} - i_{cw, in, fu}) &= \dot{m}_{cw, fu} C_{p, cw, fu} (T_{cw, o, fu} - T_{cw, in, fu}) \\ &= U_{co, fu} A_{co, fu} (LMTD)_{co, fu} \end{aligned} \quad (18)$$

Where

$$(LMTD)_{co, fu} = \frac{(T_{cw, o, fu} - T_{cw, in, fu})}{\ln \left[\frac{(T_{v, fu} - T_{cw, in, fu})}{(T_{v, fu} - T_{cw, o, fu})} \right]} \quad (19)$$

From Eq. (18) and after a few steps of simplification; the following equation is obtained:

$$(1-C)T_{cw, in, fu} + CT_{v, fu} = {}^{v, fu} T_{cw, o, fu} \quad (20)$$

Where

$$C = 1 - e^{-NTU} \quad \text{and} \quad NTU = -\frac{U_{co, fu} A_{co, fu}}{\dot{m}_{w, fu} C_{p, cw, fu}}$$

For the equilibrium correlation; the relation between the outlet brine temperature (T_b) and the condensation temperature of the vapor, (T_v), is presented by[7].

$$T_{v, fu} = T_{b, fu} - NEA - BPE \quad (21)$$

The non-equilibrium allowance (NEA) and Boiling Point Elevation (BPE) are calculated by the equations indicated in the Appendix.

4. Mathematical programming model

The main constraints of the mathematical model of the solar SSF unit were presented in the previous section. Algebraic equations are used in to the model in original form. For the iteration procedure, the outlet water temperature from the solar water heater is guessed. The

calculation procedure then marches along the solar water heater and flashing chamber. The outlet temperature of each unit is taken as an input for the next step. Finally, the outlet water temperatures are compared with the guessed inlet temperatures. The water physical properties are calculated as functions of temperature. The values of solar intensity are calculated numerically through the day and it used as an initial condition for the solution. A computer code in MATLAB® is prepared to solve the nonlinear set of equations of several variables using Gauss–Seidel iteration method.

5. Economic analysis

It is of great interest to study economically the current desalination unit because a system may be technically very efficient. However, it may not be economic; the cost of water production may be too high. The current economic analysis is conducted to determine both the cost of the water product. The total cost of ownership (TCO) concept was adopted in the analysis. The TCO concept includes different types costs like; the fixed investment costs, the production costs, the internal rate of return on investment, the operating costs, the energy costs and some other economic parameters. The investment cost of each component constituting the system is presented in Table 2.

The costs are varied from country to country depending on a lot of factors like; the labor costs, the site of the country (transportation costs), the local currency of the country and its relation to the international currency (USD).

Many assumptions are considered during the simulations as;

- Some aspects of investments are not included, like the lower probability of the systems to shutdown or proven process control is used for the desalination plants.
- All the environmental costs and the possible environmental impacts of investments are not considered.
- Costs that are not included in the capital cost estimates are: cost of drinking water conveyance facilities outside the plant boundary and interest charges during construction.
- The operating costs include the amortization or fixed charges, operating and maintenance costs and energy costs.
- A zero net salvage value is recorded (for land, buildings, equipment, etc.) and a continual replacement of such capital items into perpetuity.
- The capital cost estimate for all options is based on local prices for the equipment and no import taxes or duties are considered.
- The capital costs also include all costs for engineering, transportation, construction as well as commissioning.
- The operating and the maintenance costs are 20% of plant annual payment [12].
- Zero pretreatment costs.
- The interest rate is 5%.
- The plant life expectancy is 20 years.
- The plant availability (*f*) is 90% [12].

The calculation methodology is based on; the salvage value of the units will be zero at the end of the amortization period. The produced

fresh water can be blended with the raw water to achieve adequate potable water salinity (500 ppm according to the WHO recommended value). The amount of water that can be blended will depend on the blend water quality and the goals of the final required product water quality. For 1000 ppm brackish water, the simple mass balance results indicated that, the total produced potable water will be two times the distilled water produced, where the potable water salinity is 500 ppm. The total cost of ownership is calculated from the following relation;

$$TCO = C_{op} + C_{main} + C_{fix} \tag{23}$$

Where;

- C_{op}* is the cost of operation; it includes the energy, the operating personnel, and the handling of raw materials.
- C_{main}* is the cost of maintenance; it includes the maintenance personnel, the maintenance facility cost, the test equipment, the maintenance support and handling cost, the maintenance spares and repair parts.
- C_{fix}* is the fixed charges cost, it is calculated as follows;

$$C_{fix} = a \times C_c \tag{24}$$

Where amortization factor (**a**), which is given by [13]:

$$a = \frac{i(1+i)^n}{(1+i)^n - 1} \tag{25}$$

i, is the annual interest rate (%) and *n* is the plant life time.

C_c is the capital cost; hence the product water cost is calculated from the following relation assuming 365 working days.

$$C_{prod} = \frac{TCO}{f \times CA \times 365} \tag{26}$$

The cost of energy consumption; the electrical energy for the water pumps were 17.88 kWh/m³. The efficiency value for water pumps was 80% when calculating the consumed energy [14].

During the current study, many concerns were considered to cover the probable uncertainties like; the introduced costs are based on both a real purchasing prices and some previously mentioned assumptions. Also; all costs are adopted in a recent year (2012) in dollars, the capital cost estimate for all options was based on the Egypt local prices for the different equipments, there is no import taxes or duties are considered, finally an annual inflation rate of 5% is considered for the prices change in Egypt. In the present study, the two desalination plants modes are considered based on a thermal solar heat source only.

6. System performance assessment

In order to properly asses the feasibility of the proposed system. For example, variations in the gain output ratio. The Gained Output Ratio (GOR) is a dimensionless ratio, used for thermal desalination processes, defined either as an energy ratio or a mass ratio. As an energy ratio it is usually defined as is the ratio of the latent heat of evaporation of the water produced to the net heat input to the cycle. This parameter is, essentially, the effectiveness of water production, which is defined as an index of the amount of the heat recovery affected in the system [15]:

$$GOR = \frac{\Delta h_{evap} \dot{m}_{dis}}{\dot{Q}_{in}} \tag{27}$$

Table 2
Capital investment cost (the installation costs are included).

Item Description	Cost
Solar water heater	850 US\$
Helical coil heat exchanger	80 US\$
Flashing evaporation unit	85 US\$
Tank	10 US\$
Pumps	340 US\$
Control devices	33 US\$
Pipes, fittings	14 US\$
Accessories	6 US\$
Nano-particle kg	80 US\$

The GOR does not take into account any system efficiencies external to the desalination plant proper, such as heat losses through piping from the heat source.

7. Results and Discussion

There are five main effects of system operation parameters (feed water mass flow rate, nano-particles volume fraction, cooling water inlet temperature, feed water salinity, and cooling water mass flow rate) have a direct impacts on unit overall productivity. There are other parameters can affect in the unit productivity such as feed water salinity, wind speed and ambient temperature. But these parameters have small effects on the unit productivity, Nafey et al. [1] and Kabeel and El-Said [15]. The numerical results that presented in this section are computed for 12 hours of operation time period start at 06:00 AM until 18:00 PM on 1 August for Tanta city as shown in Fig. 4. The accumulative productivity numerically determined at the mentioned times and date according to operation conditions shown in Table 3. The solar radiation rate is computed also numerically according to location and weather conditions of Tanta city site.

7.1. Top brine temperature (TBT)

Fig. 5 shows the top brine temperature (TBT) variations as a function of solar collector working fluid mass flow rate with different nano-particle volume fraction at 12:00 AM. According to Fig. 1, it can be seen that the top brine temperature (TBT) at (3) increases with increasing of nano-particle volume fraction and decreasing with increasing of solar collector working fluid mass flow rate.

7.2. Accumulative productivity

Fig. 6 shows the fresh water accumulative production with different nano-particle volume fraction in the day time. According to the solar intensity and ambient temperature are shown in Fig. 4, it can be seen that the fresh water accumulative system production increase with the solar intensity strengthening and the freshwater production reduce with the solar intensity weakening. Also, the system productivity increase with increasing of nano-particle volume fraction. The daily water production of the system reaches about 7.7 l per one square meter of solar water heater collecting area at volume nano-particle fraction, $\varphi = 5\%$. The enhancement in productivity about 47% when use water only as a working fluid.

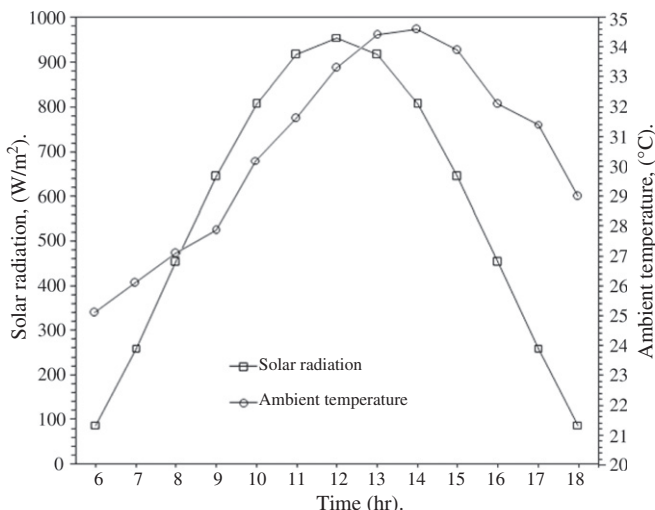


Fig. 4. Variation of solar radiation and ambient temperature during the average day time.

Table 3
Operation conditions.

$\dot{m}_{fw,ju} = 0.09$ kg/s.	$T_{cw,in} = 20$ °C.	$u_{wn} = 1.5$ m/s.	$\dot{m}_{w,bu} = \dot{m}_{fw,ju} - \dot{m}_{b,ju}$
$\dot{m}_{cw,ju} = 0.08$ kg/s	$x_{fw,in} = 2000$ ppm	$x_{cw,in} = 2000$ ppm	$\dot{m}_{nf,swc} = 14 \times 10^{-6}$ m³/s

7.3. Feed water mass flow rate effect

Variations of system productivity as a function of feed water mass flow rate are presented in Fig. 7. It shows that the increasing of the feed mass flow rate gradually, the system productivity will slowly decrease because of the decreasing in feeding water temperature of the system at constant nano-particle volume fraction.

7.4. Nano-particles volume fraction and solar collector working fluid volume flow rate effects

The variations in system productivity as a function of solar collector working fluid mass flow rate nano-particles volume fraction on the system productivity is shown in Fig. 8. It is shown that the productivity of the system increases with increasing nano-particles volume fraction. These may be explained as follows; by increasing of nano-particle volume fraction will increase the working fluid thermal conductivity, density and viscosity which increasing the solar heat gain with increasing or decreasing of heat transfer rate in helical heat exchanger as well as causes increasing or decreasing of feeding water temperature respectively. For present case, the system productivity will increase against the increasing of solar collector working fluid mass flow rate because of the decreasing in working fluid outlet temperature the solar water heater will become has effect more than increasing of heat capacity occurred by increasing of the mass flow rate of working fluid.

7.5. Cooling water mass flow rate and inlet temperature effects

The effect of the cooling water mass flow rate and inlet temperature on the system productivity is shown in Fig. 9. By increasing the cooling water mass flow rate, significant drop in the surface temperature of the condenser tubes can be achieved which results in an increase of the rate of the condensation of the water vapor on the condenser tubes surface then, the system gives higher productivity. On the other hand, the increasing the cooling water temperature, rise in the surface temperature of the condenser tubes can be achieved. So, the condensation of the

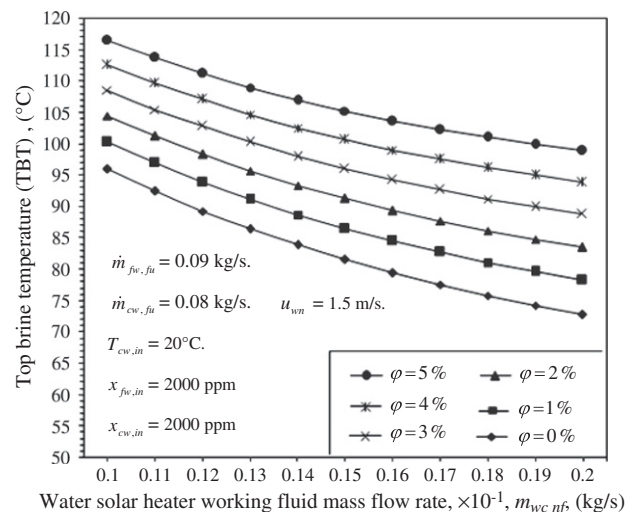


Fig. 5. Top brine temperature (TBT) variations as a function of solar collector working fluid mass flow rate with different nano-particle volume fraction at 12:00 AM.

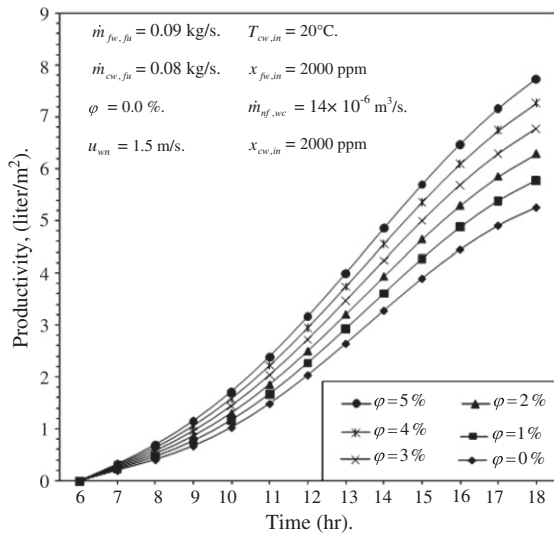


Fig. 6. Variations in system productivity as a function of nano-particle volume fraction during day hours.

water vapor on the condenser tubes surface will decrease and then lead to lower productivity. The results showed that, the water production of system increases with the decreasing of the cooling water inlet temperature and/or increasing of mass flow rate of cooling water. Moreover, the impact of decreasing of cooling water inlet temperature is more effect on system productivity than increasing of cooling water mass flow rate. The increasing in productivity about 66% for 20 °C cooling water inlet temperature.

7.6. Nu and Pr numbers

Variations in top brine temperature (TBT) as function of Nu and Pr with different nano-particle volume fraction at 12:00 AM. are presented in Fig. 10. It shows that the increasing of the TBT gradually, the Nu and Pr numbers will increase because of the increasing in the working fluid thermal conductivity.

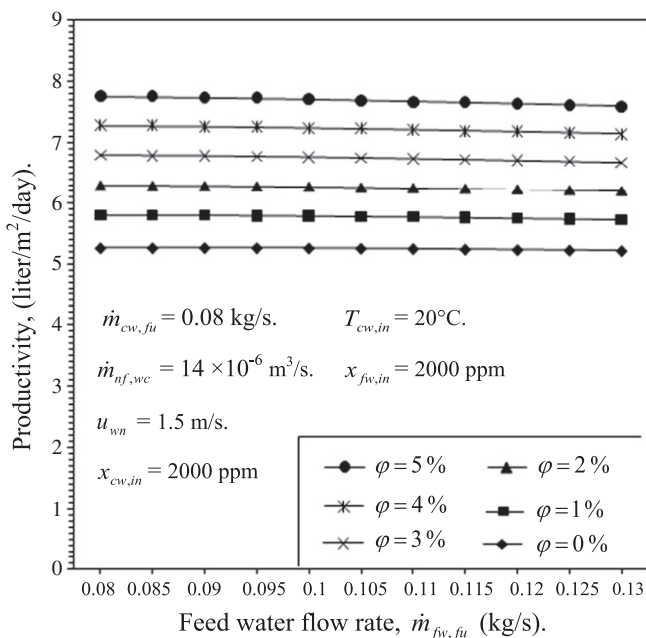


Fig. 7. Variations in system productivity as a function of feed water mass flow rate with different nano-particle volume fraction.

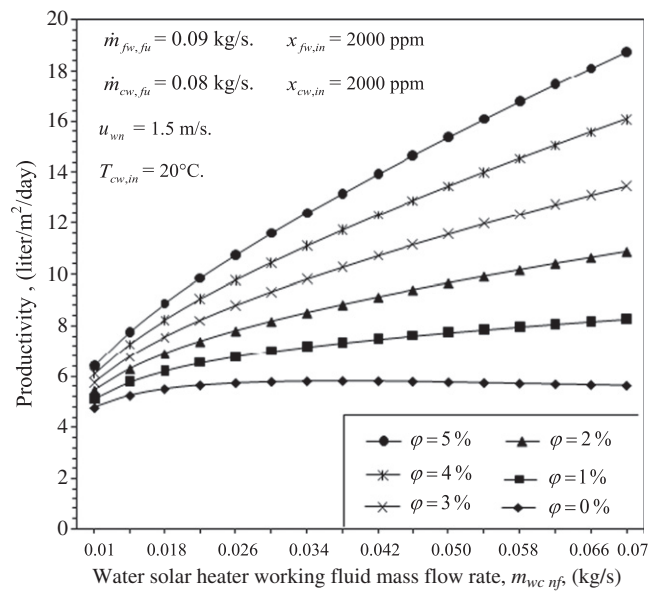


Fig. 8. System productivity variations as a function of solar collector working fluid mass flow rate with different nano-particle volume fraction.

7.7. Solar collector efficiency

Variations of solar collector efficiency (η_{wc}) variations as a function of solar collector working fluid mass flow rate with different nano-particle volume fraction at 12:00 AM.

are presented in Fig. 11. It shows that the increasing of working fluid mass flow rate and nano-particle volume fraction; the solar collector efficiency (η_{wc}) will increase.

7.8. Gain output ratio (GOR)

The efficiency of the cycle itself is measured by the gained output ratio (GOR) defined in Eq. (27). The variation in GOR as a function of

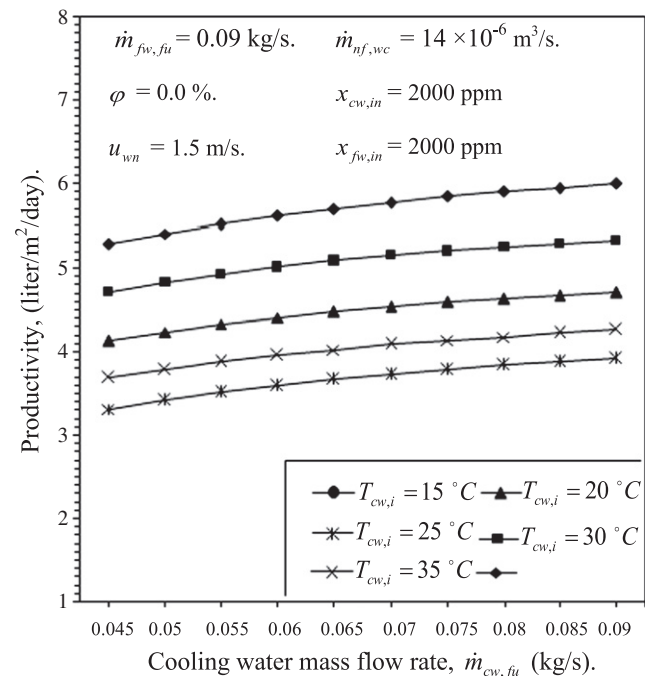


Fig. 9. Variations in system productivity as a function of cooling water mass flow rate and inlet temperature.

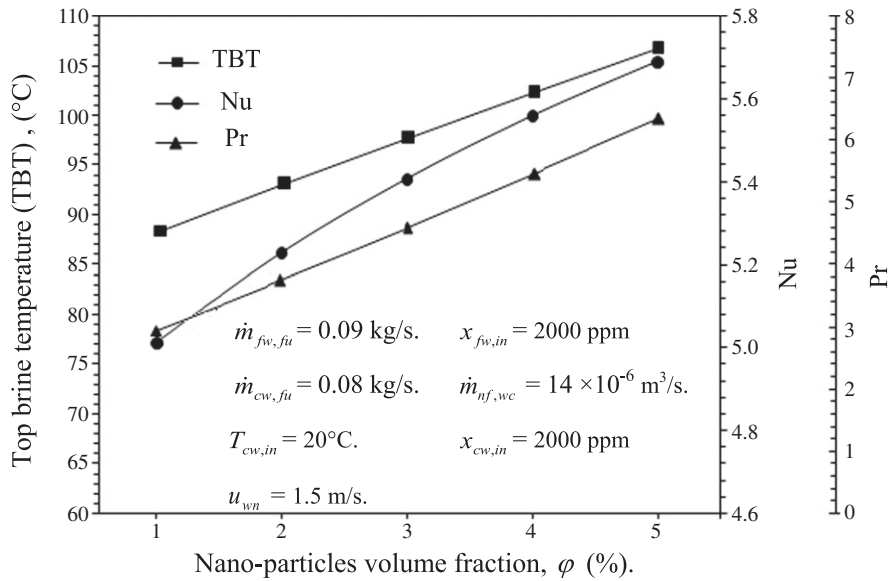


Fig. 10. Variations in top brine temperature (TBT) as function of Nu and Pr with different nano-particle volume fraction at 12:00 AM.

nano-particle volume fraction is illustrated on Fig. 12. The GOR trend of SSF unit with nano-particle volume fraction trend is non-linear; the increasing in nano-particle volume fraction causes increasing in system GOR. Gain output ratio reaches about 1.058 at φ equal 5% 1.045.

7.9. Effect of water solar heaters collecting areas on water cost and system productivity

The effects of water solar heaters collecting area on the cost of the water and system productivity are shown through Fig. 13. It is shown that the increase of the water solar heater collecting area causes an increase in the fresh water productivity. This increase in fresh water productivity appreciably decreases the fresh water production cost. That reduction in cost is due to; the increase in the amount of heat absorbed by salt water, hence the increase in fresh water productivity which has a significant influence on water cost calculation. From another point of

view, the increase of the water solar heater collecting area requires increases in the fixed capital cost. These two opposite factors effects on the fresh water productivity cost should be optimized. The current results indicated that; the increase in the collecting area of the solar water heater could decrease the fresh water cost by 63.3% with an increase in the fixed capital cost by 87%. Also, the optimum solar water heater collecting area gives high productivity and low cost equal about 3.54 m².

The investment cost of the entire unit, determined by summing the investment cost of each unit components, is 1417 US\$. The results show that the system gives fresh water with cost 16.43 US\$ at 7.075 m² solar air water heater collecting area which accepted compared with other technologies [8,16,17]. The pumping power was supplied using an external electrical power supply which had a high running cost and cannot be formed into a desirable size easily. In order to overcome these drawbacks, the pumps power can be reduced by coupling to stand-alone PV system and storage batteries and using passive vacuum tower instead of

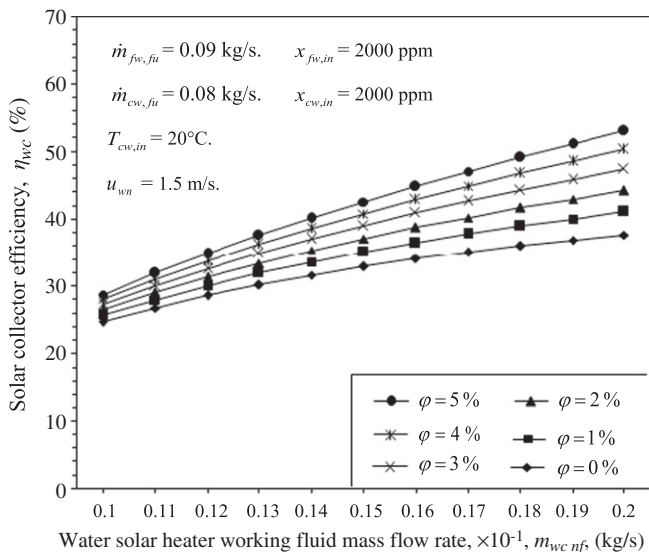


Fig. 11. Solar collector efficiency (η_{wc}) variations as a function of solar collector working fluid mass flow rate with different nano-particle volume fraction at 12:00 AM.

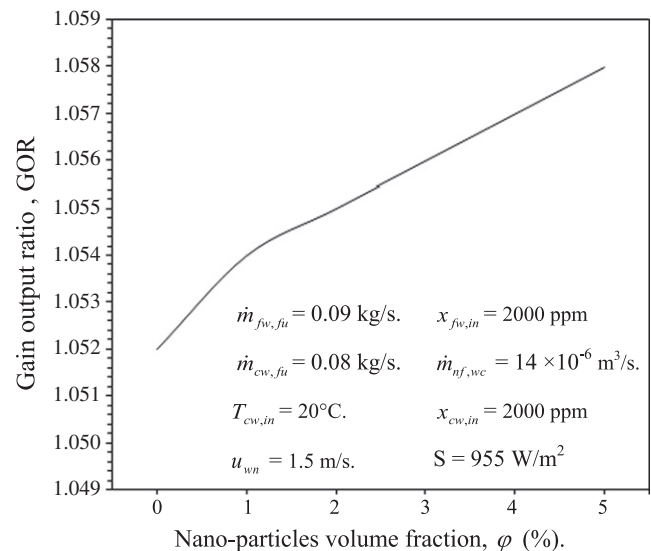


Fig. 12. Variations in gain output ratio (GOR) as function of nano-particle volume fraction.

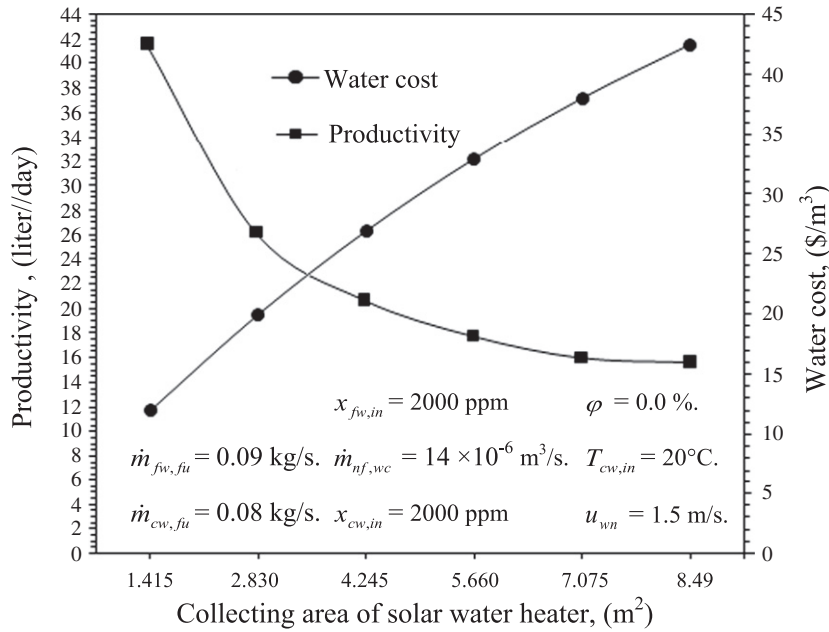


Fig. 13. Variations in system productivity and water cost as a function of collecting area of solar water heater.

external electrical power and vacuum pump respectively. The using of PV panels and passive vacuum tower will be increasing the capital cost by at most 10200 US\$. This will eliminate the energy cost and increase the water cost by at most 31.13 US\$/m³ according to 2012 prices in Egypt.

7.10. Effect of nano-particle volume fraction on water cost and system productivity

The effects of nano-particle volume fraction on the cost of the water and system productivity are shown through Fig. 14. According to the results explanation in Section (7.4), it is shown that the water cost is affect by system productivity and nano-particle volume fraction. The water cost reaches 11.68 \$/m³ at φ = 5%.

8. Model results validation

The main components of the program are validated separately with other published works. The present results are generally in agreement

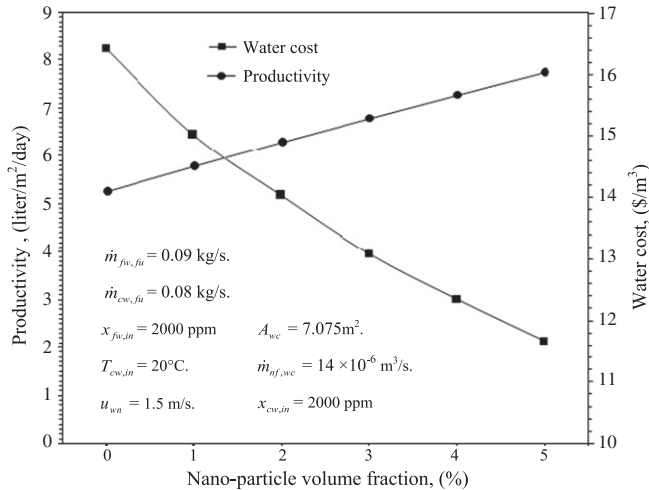


Fig. 14. Variations in system productivity and water cost as a function of nano-particle volume fraction.

with the trend of Matuska et al. [18] and Nafey et al. [1] for solar collector and SSF unit respectively. In addition, experimental replication of the proposed system is currently underway to validate model assumptions and predictions.

9. Conclusion

A numerical investigation was carried out with the objective of studying a single stage flashing evaporation unit. An estimation of the desalted water production and cost is done.

The possible factors and parameters those have an effect on the system production and cost are studied.

Five main parameters that have influence on the system productivity are the feed water mass flow rate, nano-particles volume fraction, cooling water inlet temperature, feed water salinity, and cooling water mass flow rate. The main conclusions are summarized:

1. The flashing desalination technology with similar construction design considerations of commercial multi-stage flashing (MSF) can be applicable for small scale needs with daily fresh water productivity up to 7.7 l/m²/day.
2. The volume fractions of nano-particle in solar collector working fluid have a significant impact on increasing the fresh water production and decreasing cost.
3. The system production can be increased by increasing cooling water flow rate and decreasing its temperature.
4. The estimated cost of the potable water produced is about 11.68 US \$/m³.
5. The SSF system gain output ration GOR was 1.058.
6. The collecting area of solar water heater has significant effect on the reduction of the fresh water production cost.
7. The fresh water production cost decreases with the increase in the solar water heater collecting area.
8. The optimum solar water heater collecting area gives high productivity and low cost equal about 3.54 m².
9. The increase in collecting area of the solar water heater effect could reduce the water production costs by 63.3% with an increase in the fixed capital cost by 87%.

Nomenclatures

Latin Symbols

A	area, m^2
q	energy gain, W/m^2
C_p	specific heat, J/kgK
x	water salinity, ppm
g	gravitational constant, m^2/s
e	absorber plate to cover spacing and absorber plate to back plate spacing, m
D	Diffusivity coefficient, m^2/s
h	heat transfer coefficient, W/m^2K
Re	Reynolds number $\equiv \frac{\rho u d}{\mu}$, dimensionless
I	solar radiation rate, W/m^2
d	diameter, m
H	height, m
L	length, m
W	width, m
K	thermal conductivity, W/mK
F_R	collector heat removal factor, dimensionless
S	actual absorbing radiation solar energy, W/m^2
Pr	Prandtl number $\equiv \frac{C_p \mu}{K}$, dimensionless
U	heat loss coefficient, W/m^2K
\dot{m}	Mass flow rate, kg/s
Ra	Rayleigh number $\equiv \frac{C_p \mu}{K}$, dimensionless
u	velocity, m/s
p	pressure, N/m^2
T	Temperature, K or $^{\circ}C$
F'	Collector efficiency factor, dimensionless
F	fin efficiency, dimensionless

Greek Symbols

α	solar absorptance of collector plate, dimensionless
α'	thermal diffusivity, m^2/s
β	collector tilt angle, degree
β'	volumetric coefficient of expansion, K^{-1}
ν	kinetic viscosity, m^2/s
ε'	emittance factor
μ	dynamic viscosity, $kg/m.s$
ρ	density, kg/m^3
σ	Stefan–Boltzmann constant = $5.67 \times 10^{-8} W/m^2K^4$.
τ	solar transmittance of glazing
δ	thickness, m
φ	volume fraction of Cu, $m^3 (Cu)/m^3$ (distilled water).

Subscripts

1	object 1
2	object 2
w	water
h	hydraulic
bu	backup
rb	rejected brine
wc	water solar collector
c	convection
t	top
am	ambient
o	out
r	radiation
in	in
p	heat-absorbing plate
lb	local base

b	bottom
bi	back insulation
e	edge
u	useful
row	row
m	mean
L	overall
v	vapor
cf	condensate film
gc	glass cover
bo	bond
hot	hot
$cold$	cold
$loss$	loss
sw	sea water
iw	inside wall
cf	condensate film
cw	cooling water
sr	surface
wn	wind
T	total
dis	distillate
fin	fin
ap	Aperture
fu	flashing unit
bp	brine pool
$conv$	conventional
lm	log mean
eq	equilibrium
nf	nanofluid
bf	base fluid
np	nanoparticle

Appendix

- Convective heat transfer coefficient through a water flowing inside the tubes.

In the laminar regime, the recommended correlation for predicating the average film coefficient is, [19]:

$$h_{cw,iw,co} = 1.86 \left(\frac{K_{w,co}}{d_{tube,in,co}} \right) \left(Re_{di} Pr \frac{d_{tube,in,co}}{L_{tube,co}} \right)^{\frac{1}{3}} \left(\frac{\mu_{w,co}}{\mu_{w,tube,in,co}} \right)^{0.14} \quad \text{for } Re_{di} < 2300.$$

$$h_{cw,iw,co} = 0.116 \left(\frac{K_{w,co}}{d_{tube,in,co}} \right) \left(Re_{di}^{2/3} - 125 \right) Pr^{1/3} \left[1 + \left(\frac{d_{tube,in,co}}{L_{tube,co}} \right)^{2/3} \right] \left(\frac{\mu_{w,co}}{\mu_{w,tube,in,co}} \right)^{0.14} \quad \text{for } 2300 \leq Re_{di} \leq 10^4$$

$$h_{cw,iw,co} = \frac{0.023 K_{w,co} Pr^n Re_{di}^{0.8}}{d_{tube,in,co}} \quad \text{for } Re_{di} > 10^4, 0.7 < Pr < 100, \text{ and } L_{tube}/d_i > 60.$$

Where

$$n = \begin{cases} 0.4, & T_{tube,in} > T_{bulk} \text{ (cooling)} \\ 0.3, & T_{tube,in} < T_{bulk} \text{ (heating)} \end{cases}$$

- Liquid condensed film heat transfer coefficient. This coefficient is given by the Nusselt correlation [20]:

$$h_{cf,co} = 0.729 \left[\frac{K_{w,co}^3 \rho_{w,co} (\rho_{w,co} - \rho_{v,co}) g \lambda_{fg,co}^*}{\mu_{w,co} d_{tube,o,co} (T_{s,co} - T_{tube,o,co})} \right]^{0.25}$$

For $(N_{Ps,tube,co})$, vertically aligned: $h_{cf,co}|_{N_{Ps,tube,co}} = h_{cf,co} N_{Ps,tube,co}^{-0.25}$

- Heat transfer coefficients of water heater.

The convection heat transfer coefficient due to wind is recommended by [21]

$$h_{wn} = 5.7 + 3.8u_{wn} \quad \text{for } 0 \leq u_{wn} \leq 7 \text{ m/s.}$$

- The radiation heat transfer coefficient

$h_{r,1-2} = \frac{\sigma(T_1+T_2)(T_1^2+T_2^2)}{\frac{1}{\epsilon_1} + \frac{A_1}{A_2}(\frac{1}{\epsilon_2}-1)}$ Where $(T_1, T_2, \epsilon_1, \epsilon_2, A_1, A_2)$ are the temperatures, The convection heat transfer coefficients for the fluid moving on the absorbing plate and on the bottom plate are recommended by [22] as:

$h_{c,p-f} = h_{c,b-f} = \left(\frac{K_a a}{d_h}\right) \times 0.0158 \text{Re}_{d_h}^{0.8}$ where (Re_{d_h}) is defined as follows, $\text{Re}_{d_h} = \frac{\rho_a \bar{u}_f d_h}{\mu_a}$ in which \bar{u}_f (m/s) is the mean velocity of fluid in the channel.

The hydraulic diameter (d_h) is defined as follows:

$$d_h = \frac{4 \times \text{flow cross sectional area}}{\text{watted perimeter}} = \frac{4W_p e}{2W_p} = 2e$$

- **The convection heat transfer coefficient between the glass cover and the absorbing plate** is calculated by [23]:

$$h_{c,p-g2} = \frac{K_a Nu_a}{e}$$

Where

$$Nu_a = 1 + 1.446 \left[1 - \frac{1708}{Ra_a \times \cos(\beta)} \right]^+ \left\{ 1 - \frac{1708 [\sin(1.8\beta)]^{1.6}}{Ra_a \times \cos(\beta)} \right\} + \left\{ \left[\frac{Ra_a \times \cos(\beta)}{5830} \right]^{0.333} - 1 \right\}^+$$

Where the plus sign in the superscript means that only positive values of the terms in the square brackets are to be used (i.e., use zero if the term is negative). This correlation is valid for tilt collector angle $0 \leq \beta \leq 75$.

$$Ra_a = \frac{g\beta' Pr_a}{\nu^2} (T_p - T_{g2}) E_{p,as}^3 \quad Pr_a = \frac{\nu_a}{\alpha_a} \quad \text{and} \quad \alpha'_a = \frac{K_a}{\rho_a C_{p,a}}$$

For ideal gas, $\beta' = 1/T$ (K^{-1})

- **The top loss coefficient** from the collector absorber plate to the ambi-ent is given by the following empirical equation, [11]:

$$U_t = \left\{ \frac{N_{gc}}{\frac{C}{T_p} \left[\frac{T_{p,m} - T_{am}}{N_{gc} + f} \right]^e} + \frac{1}{h_{wn}} \right\}^{-1} + \frac{\sigma(T_{p,m} + T_{am})(T_{p,m}^2 + T_{am}^2)}{\left(\epsilon'_p + 0.0059 N_{gc} h_{wn} \right)^{-1} + \frac{2N_{gc} + f - 1 + 0.13\epsilon'_p}{\epsilon'_{gc}} - N_{gc}}$$

Where

$$C = 520 \left(1 - 0.000051\beta^2 \right) \text{ for } 0^\circ < \beta < 70^\circ; \text{ for } 70^\circ < \beta < 90^\circ, \text{ use } \beta = 70^\circ$$

$$f = \left(1 + 0.089h_{wn} - 0.1166h_{wn}\epsilon'_p \right) \left(1 + 0.07866N_{gc} \right) \text{ and}$$

$$e = 0.43 \left(1 - \frac{100}{T_{p,m}} \right) T_{p,m}(K),$$

The range of conditions over which above equation has been develop, is follows, [24]:

$$\begin{aligned} 320 &\leq T_{p,m} \leq 420 \text{ K} \\ 320 &\leq T_{p,m} \leq 420 \text{ K} \\ 320 &\leq T_{p,m} \leq 420 \text{ K} \\ 260 &\leq T_{am} \leq 310 \text{ K} \\ 0.1 &\leq \epsilon'_p \leq 0.95 \\ 0 &\leq u_{wn} \leq 10 \text{ m/s} \\ 0 &\leq \beta \leq 90 \text{ K} \\ 1 &\leq N_{gc} \leq 3 \end{aligned}$$

- **The bottom energy loss coefficient** (U_b) is given by:

$$U_b = \frac{K_{bi}}{\delta_{bi}}$$

- **The edge loss coefficient**-area product is $(UA)_e$ then the edge loss coefficient, based on the collector area (A_{wc}) [11] is:

$$U_e = \frac{(UA)_e}{A_{wc}} = \frac{K_e A_e}{\delta_e A_{eff}}$$

- **The overall heat loss coefficient** is a complicated function of the collector construction and its operating conditions, given by the following expression:

$$U_{L,wc} = U_t + U_b + U_e$$

- **Boiling Point Elevation**

The correlation for the boiling point elevation of seawater is [12].

$$\begin{aligned} \text{BPE} &= \left(a_1 x^1 + a_2 x + a_3 x^3 \right) \times 10^{-4} \\ a_1 &= 8.325 \times 10^{-2} + 1.883 \times 10^{-4} T_b + 4.02 \times 10^{-6} T_b^2 \\ a_2 &= -7.625 \times 10^{-4} + 9.02 \times 10^{-5} T_b - 5.2 \times 10^{-7} T_b^2 \\ a_3 &= 1.522 \times 10^{-4} - 3 \times 10^{-6} T_b - 3 \times 10^{-8} T_b^2 \end{aligned}$$

Where T_b is the brine temperature in $^\circ\text{C}$ and x is the salt concentration. The above equation is valid over the following ranges: $10000 \leq x \leq 20000 \text{ ppm}$, $10 \leq T \leq 110 \text{ }^\circ\text{C}$.

- **Non-Equilibrium Allowance**

The correlations for the non-equilibrium allowance (NEA) for the MSF system is developed through the following equation give value for NEA [$^\circ\text{C}$] as a function of the chamber length, brine pool height, the water film velocity, and water film temperature drop [3];

$$NEA = \text{erf} \left[\left(\frac{H_{bp}}{2} \sqrt{\frac{\rho_{fw} C_{p, fw}}{a_1 \cdot L_{fu} / u_{wf}}} \right)^{a_2} \right]$$

Where

$$\begin{aligned} a_1 &= 5.43 \times 10^3 \cdot H_{bp}^{0.778} \cdot \rho_v^{0.558} \quad a_2 = 0.565 \Delta T_{su}^{0.181}, \\ a_2 &= 0.565 \Delta T_{su}^{0.181} \quad \text{and} \quad u_{wf} = \frac{\dot{m}_{fw}}{\rho_{fw} W_{fu} H_{bp}}, \end{aligned}$$

Superheat (ΔT_{su}) represents the theoretically maximum temperature drop of water film in a given flash system and therefore is viewed as the driving force for flash phenomena

$$\Delta T_{su} = T_{fw} - T_{eq} \text{ or } \Delta T_{su} = T_{wf} - T_{eq} \text{ and } T_{eq} = T_s(p_{eq}).$$

•Heat transfer coefficient of the nano-fluid

The heat transfer coefficient of the nano-fluids is calculated from the following equations, [25].

$$Nu_{nf} = \frac{h_{nf}d_i}{K_{nf}} \text{ and } h_{nf} = \frac{K_{nf}Nu_{nf}}{d_i}$$

For laminar flow

$$Nu_{nf} = 0.4328 \left(1.0 + 11.285\varphi^{0.754} Pe_d^{0.218} \right) Re_{nf}^{0.333} Pr_{nf}^{0.4}$$

For turbulent flow

$$Nu_{nf} = 0.0059 \left(1.0 + 7.6286\varphi^{0.6886} Pe_d^{0.001} \right) Re_{nf}^{0.9238} Pr_{nf}^{0.4}$$

The sample nano-fluid used to predict the above correlations was de-ionized water with a dispersion of Cu particles with below 100 nm diameter.

$$Pe_d = \frac{u_m d_{np}}{\alpha'_{nf}}, \quad Re_{nf} = \frac{u_m d_i}{\nu_{nf}}, \text{ and } Pr_{nf} = \frac{\nu_{nf}}{\alpha'_{nf}}$$

To calculate this parameter, the thermal diffusivity of the nano-fluid an α'_{nf} is defined as

$$\alpha'_{nf} = \frac{K_{nf}}{\rho_{nf} C_{p,nf}}$$

•Properties of Nanofluid

The following equations are used for calculating the thermophysical properties of nano-fluid [26].

Density

The nano fluid density is the average of the nano-particles and base fluid densities as follow.

$$\rho_{nf} = (1-\varphi)\rho_{bf} + \varphi\rho_{np}$$

In above equation the nano-particles and base fluid densities are in kg/m³.

Specific heat

$$C_{p,nf} = (1-\varphi)C_{p,bf} + \varphi C_{p,np}$$

In above equation the nano-particles and base fluid specific heats are in J/kg.K.

Dynamic viscosity

$$\mu_{nf} = \mu_{bf} \left(533.9\varphi^2 + 39.11\varphi + 1 \right)$$

In above equation the nano-particles and base fluid viscosities are in kg/m.s.

Kinematics viscosity

$$\nu_{nf} = \frac{\mu_{nf}}{\rho_{nf}}$$

Thermal conductivity

According to the Maxwell model for thermal conductivity for solid-liquid mixtures, the nano fluid thermal conductivity, (K_{nf}), is given by, [27]:

$$K_{nf} = K_{bf} \left[\frac{K_{np} + 2K_{bf} + 2\Phi(K_{np} - K_{bf})}{K_{np} + 2K_{bf} - \Phi(K_{np} - K_{bf})} \right]$$

In above equation the all thermal conductivities are in W/m.K.

References

- [1] A.S. Nafey, M.A. Mohamad, S.O. El-Helaby, M.A. Sharaf, Theoretical and experimental study of a small unit for solar desalination using flashing process, *Energy Convers. Manag.* 48 (2007) 528–538.
- [2] H. Baig, M.A. Antar, S.M. Zubair, Performance characteristics of a once-through multi-stage flash distillation process, *Desalin. Water Treat.* 13 (2010) 174–185.
- [3] Y. Junjie, Z. Dan, C. Daotong, W. Guifang, L. Luning, Experimental study on static/circulatory flash evaporation, *Int. J. Heat Mass Transf.* 53 (2010) 5528–5535.
- [4] M. Saad, M. Ahmed, V.M. Morcos, Performance analysis of a vacuum desalination system, *Proceedings of the ASME International Mechanical Engineering Congress & Exposition, Denver, Colorado, USA, 2011.*
- [5] M. Abutayeh, D.Y. Goswami, Solar Flash Desalination Under Hydrostatically Sustained Vacuum, *J. Sol. Energy Eng.* 131 (2009) 1–7.
- [6] L.G. Asirvatham, N. Vishal, S.K. Gangatharan, D. Mohanlal, Experimental Study on Forced Convective Heat Transfer with Low Volume Fraction of CuO Water Nanofluid, *Energies* 2 (2009) 97–119.
- [7] T. Yousefi, F. Veysi, E. Shojaezadeh, S. Zinadini, An experimental investigation on the effect of Al₂O₃-H₂O nanofluid on the efficiency of flat-plate solar collectors, *Renew. Energy* 39 (2012) 293–298.
- [8] F. Banat, N. Jwaied, Economic evaluation of desalination by small-scale autonomous solar-powered membrane distillation units, *Desalination* 220 (1) (2008) 566–573.
- [9] A.E. Kabeel, T. Abou Elmaaty, Emad M.S. El-Said, Economic analysis of a small-scale hybrid air HDH-SSF (humidification and dehumidification- water flashing evaporation) desalination plant, *Energy* 53 (2013) 306–311.
- [10] Abdel Nasser A. Mabrouk, Techno-economic Analysis of Once through Long Tube MSF Process for High Capacity Desalination Plants, *Desalination* 317 (2013) 84–94.
- [11] J.A. Duffie, W.A. Beckman, *Solar Engineering of Thermal Processes*, 3rd edition John Wiley, Toronto, 2006.
- [12] H.T. El-Dessouky, H.M. Ettouney, *Fundamentals of Salt water Desalination*, 1st edition ELSEVIER, 2002.
- [13] Y. Jaluria, *Design and optimization of thermal systems*, 2nd edition CRC Presses, 2007. 398.
- [14] A. Eslamimanesh, M.S. Hatamipour, Economical study of a small-scale direct contact humidification-dehumidification desalination plant, *Desalination* 250 (1) (2010) 203–207.
- [15] A.E. Kabeel, M.S. Emad, A. El-Said, hybrid solar desalination system of air humidification-dehumidification and water flashing evaporation: Part I. A numerical investigation, *Desalination* 320 (2013) 56–72.
- [16] J. Rheinlaender, F. Graeter, Technologies for desalination of typically 10 m³ of water per day, *Desalination* 139 (2001) 393–397.
- [17] S. Bouguecha, B. Hamrouni, M. Dhahbi, Small scale desalination pilots powered by renewable energy sources: case studies, *Desalination* 183 (1) (2005) 151–165.
- [18] T. Matuska, V. Zmrhal, J. Metzger, Detailed modeling of solar flat – plate collectors with design tool KOLEKTOR 2.2, Eleventh International IBPSA Conference Glasgow, Scotland, July 27–30, 2009.
- [19] F.C. McQuiston, Jerald D. Parker, Jeffrey Spitler, *Heating Ventilating and Air Conditioning Analysis and Design*, 6th edition John Wiley & Sons, Inc., 2005
- [20] ASHRAE, *Fundamental Handbook*, 2009.
- [21] W.H. McAdams, *Heat Transmission*, 3rd edition McGraw-Hill, New York, 1954.
- [22] W.M. Kays, M.E. Crawford, *Convective Heat and Mass Transfer*, 2nd edition McGraw – Hill, New York, 1980. 213.
- [23] K.G.T. Hollands, T.E. Unny, G.D. Raithby, L. Konicek, Free convection heat transfer across inclined air layers, *J. Heat Transf.* 189 (1976).
- [24] H. Kazeminejad, Numerical analysis of two dimensional parallel flow flat-plate solar collectors, *Renew. Energy* 26 (2002) 309–323.
- [25] W. Daungthongsuk, S. Wongwises, A critical review of convective heat transfer of nano-fluids, *Renew. Sust. Energ. Rev.* 11 (5) (2007) 797–817.
- [26] L.S. Sundar, K.V. Sharma, Numerical Analysis of Heat Transfer and Friction Factor in A Circular Tube with γ -Al₂O₃ Nano-fluid, *Dyn. Fluids* 4 (2) (2008) 121–129.
- [27] X. Wang, A.S. Mujumdar, Heat transfer characteristics of nano-fluids: a review, *Therm. Sci.* 46 (2007) 1–19.